

Multivariate Information Theory Uncovers Synergistic Subsystems of the Human Cerebral Cortex

Thomas F. Varley,^{1,2,*} Maria Pope,^{2,3,*} Joshua Faskowitz,¹ and Olaf Sporns^{1,2,3,4}

¹*Department of Psychological and Brain Sciences, Indiana University, Bloomington, IN 47405*

²*School of Informatics, Computing & Engineering, Indiana University, Bloomington, IN 47405[†]*

³*Program in Neuroscience, Indiana University, Bloomington, IN 47405*

⁴*Indiana University Network Science Institute, Indiana University, Bloomington, IN 47405*

(Dated: June 15, 2022)

One of the most well-established tools for modeling the brain as a complex system is the functional connectivity network, which examines the correlations between pairs of interacting brain regions. While powerful, the network model is limited by the restriction that only pairwise dependencies are visible and potentially higher-order structures are missed. In this work, we explore how multivariate information theory can reveal higher-order, synergistic dependencies in the human brain. Using the O-information, a measure of whether the structure of a system is redundancy- or synergy-dominated, we show that synergistic subsystems are widespread in the human brain. We provide a mathematical analysis of the O-information to locate it within a larger taxonomy of multivariate complexity measures. We also show the O-information is related to a previously established measure, the Tononi-Sporns-Edelman complexity, and can be understood as an expected difference in integration between system scales. Highly synergistic subsystems typically sit between canonical functional networks, and may serve to integrate those networks. We then use simulated annealing to find maximally synergistic subsystems, finding that such systems typically comprise ≈ 10 brain regions, also recruited from multiple canonical brain systems. Though ubiquitous, highly synergistic subsystems are invisible when considering pairwise functional connectivity, suggesting that higher-order dependencies form a kind of “shadow structure” that has been unrecognized by established network-based analyses. We assert that higher-order interactions in the brain represent a vast and under-explored space that, made accessible with tools of multivariate information theory, may offer novel scientific insights.

Keywords: Functional connectivity, higher-order interaction, information theory, synergy, redundancy, mutual information, brain, fMRI, network science.

SIGNIFICANCE STATEMENT

Network models of the brain have emerged as among the most powerful tools for understanding its structure and function. Recently, neuroscientists and complexity scientists have begun studying higher-order interactions between multiple brain regions that cannot be easily modeled as a network. In this paper, we use multivariate information theory to show that the brain has a large number of higher-order, synergistic subsystems that are invisible when considering a pairwise graph structure. We analytically relate these synergies to mathematical notions of complexity and show how the brain can be understood as a complex system combining elements of integration, segregation, synergy, and redundancy. The space of higher-order dependencies represents a large, unexplored territory for neuroscience research.

INTRODUCTION

Perhaps the most ubiquitous model used in complex systems is the *network*, comprising pairwise interactions between different elements of the system as directed or undirected graphs [1, 2]. While network models can be extremely powerful, they are also fundamentally limited by the constructional rule that every interaction between elements is strictly bivariate. Hence, interactions between three or more nodes must be indirectly inferred, using methods such as motifs [3], transitivity or clustering coefficients [4], and mapping cores or mesoscale communities [5, 6]. Increasingly, statistical interactions involving more than two elements (termed “higher-order” interactions) are recognized to be a key feature of complex systems [7, 8], making the task of recognizing and modeling higher-order structures an important, developing field. However, a lack of well-developed, formal tools, as well as the inherent computational and combinatorial difficulties associated with higher-order interactions have limited their application. In neuroscience, higher-order interactions have been theoretically implicated as building blocks of complexity [9, 10] and functional integration [11]. Empirically, they have been found at multiple scales, including in neuronal networks [12–17], electrophysiological signals [18, 19], and fMRI BOLD data [20–

* These authors contributed equally.

[†] tvarley@indiana.edu

22], where higher-order interactions have been proposed to relate to emergent mental phenomena and consciousness [23].

Recently, Rosas and Mediano [24] proposed that information theory could be used to identify higher-order interactions in multivariate systems, and furthermore, that it is possible to disentangle qualitatively different *kinds* of interactions, characterized by pairwise *redundant* and *synergistic* modes of information sharing. Intuitively, redundant information corresponds to information that is “copied” over many different elements such that the observation of a single element resolves the corresponding uncertainty in all of the other elements. In contrast, synergistic information sharing occurs when uncertainty can only be resolved by considering the *joint state* of two or more variables. This space of redundant and synergistic interactions in the brain remains largely unexplored, as it comprises interactions that are typically inaccessible to a bivariate, functional connectivity network analysis. Synergy is of potential interest because it tracks the ability of the brain to generate *novel* information through the interactions of multiple brain regions (sometimes called information “modification”) [25]. In studies of cortical neural networks, synergy has been associated with neural “computation” (the genesis of new information through a non-trivial interaction of multiple inputs) [12–16]. The pure synergy itself is hard to calculate, however (requiring super-exponential computing time for even modestly sized systems), prompting a search for scalable heuristic measures of redundancy/synergy bias. Rosas et al. introduced the O-information [24] as such a measure, which gives an overall estimate of the extent to which a system is redundancy *dominated* or synergy *dominated*, with negative O-information indicating the presence of predominantly synergistic interactions. Despite strong appeal as a quantitative metric related to computation the origins and neural manifestations of O-information have remained elusive, if not “enigmatic” [26].

In this work, we apply a range of information-theoretic measures to resting state fMRI data acquired from human cerebral cortex with the aim to identify ensembles of regions (subsystems) that express specific modes of higher-order statistical dependencies. First, we introduce the mathematical machinery required to derive the O-information, and its interpretation in the context of multivariate information sharing processes. We disclose an analytic relationship of O-information to other, more well-known multivariate metrics such as the Tononi-Sporns-Edelman complexity [10]. Next, we apply multivariate information metrics to brain data and uncover the presence of abundant and widely distributed subsystems expressing synergy (negative O-information) across the entire cerebral cortex. Finally, we discuss what our insights reveal about the structure and functional roles of higher-order relations in brain activity.

I. THEORY

A. Integration, Segregation, Redundancy, Synergy

A fundamental idea in modern theoretical neuroscience states that the nervous system maintains a balance between “integration” and “segregation” [9]. The integration-segregation balance principle is based on the insight that the nervous system combines regional elements of functional specialization, with system-wide functional integration. Considerable empirical work has gone into the neural integration-segregation hypothesis, and the on-going balance of integrated and segregated dynamics has been found to be regulated by distinct neuromodulatory systems [27, 28], and correlates with conscious awareness [29, 30].

The segregation-integration spectrum is typically visualized as a one-dimensional space: on one extreme the system is totally dis-integrated and every element is behaving entirely independently of all the others. On the other extreme is the case of total integration: every element synchronizes with every other element so that the whole system is densely connected. In the middle there is a “complex” regime where the system combines elements of independence and integration. As it was originally formulated, integration and segregation were discussed in the contexts of networks, and higher-order interactions were inferred via partitioning the system into subsets of varying numbers of nodes [9]. These arguments pre-dated the rigorous, mathematical distinction between redundancy and synergy, introduced in the work of Williams and Beer almost two decades later [31]. Building on these foundations, as well as the definition of O-information from Rosas et al., [24], we argue that the notion of integration can be expanded to include *redundant integration* and *synergistic integration*, resulting in a more complex space described by distinct dimensions of integration, segregation, redundancy, and synergy (although these do not form an orthogonal basis). This high-dimensional, qualitative configuration space may be viewed as an informational “morphospace” [32–34] and provides a framework for the detailed comparison of different systems.

B. Information Theory and Higher-Order Information-Sharing

In this section, we introduce the basics of information theory necessary to understand its application to higher-order relationships. For a more thorough introduction, readers may be interested in Cover & Thomas [35]. The basic object of study in information theory is the *entropy* [36], which quantifies the uncertainty that we, as observers, have about the state of a variable X . If the states of X are drawn according to the probability distribution $P(X = x)$ with Support Set \mathcal{X} , then the entropy of X is:

$$H(X) = - \sum_{x \in \mathcal{X}} P(x) \log_2 P(x) \quad (1)$$

Now consider two variables X_1 and X_2 : how does knowing the state of X_1 reduce our uncertainty (the entropy) about the state of X_2 ? The answer is given by the mutual information [36], which can be written in two mathematically equivalent forms:

$$\begin{aligned} I(X_1; X_2) &= H(X_1) + H(X_2) - H(X_1, X_2) \\ &= H(X_1, X_2) - [H(X_1|X_2) + H(X_2|X_1)] \end{aligned} \quad (2)$$

The bivariate mutual information is often applied in the study of complex systems for the inference of functional connectivity networks (e.g. [37–40]), which can reveal the structure of dyadic interactions between different elements [41]. While functional connectivity networks are extremely powerful, they are fundamentally limited by their pairwise structure and are insensitive to “higher-order” interactions between two or more variables.

The natural place to begin an analysis of higher-order structures in neural data, then, is by attempting to generalize the mutual information to account for more than two variables. Unfortunately, there is no single unique generalization, and at least three are known to exist: the total correlation, the dual total correlation, and the interaction/co-information (which we will not address here) [35]. The *total correlation*, (also referred to as the “integration” in [9]) is formally a straightforward generalization of Eq. 2:

$$TC(\mathbf{X}) = \sum_{i=1}^N H(X_i) - H(\mathbf{X}) \quad (4)$$

$$= D_{KL}(P(X_1, \dots, X_N) || \prod_{i=1}^N P(X_i)) \quad (5)$$

Where \mathbf{X} is a “macro-variable” comprised of an ensemble of multiple random variables: $\mathbf{X} = \{X_1, X_2, \dots, X_N\}$ and $D_{KL}()$ is the Kullback-Leibler divergence. The total correlation is low when every variable is independent, and high when every variable is individually highly entropic but the joint-state of the whole has low entropy. This occurs when the whole system is dominated by *redundant* interactions: the state of a single variable discloses a large amount of information about the state of every other variable.

The second generalization of mutual information is the *dual total correlation*, formally a generalization of Eq. 3:

$$DTC(\mathbf{X}) = H(\mathbf{X}) - \sum_{i=1}^N H(X_i | \mathbf{X}^{-i}) \quad (6)$$

where $H(X_i | \mathbf{X}^{-i})$ refers to the *residual entropy* [42]: the uncertainty intrinsic to the i^{th} element of \mathbf{X} that is

not resolved by any other variable, or collection of variables in \mathbf{X} . The difference between the joint entropy and the sum of the residual entropies is all the entropy that is “shared” between at least two elements of \mathbf{X} (i.e. is redundantly common to two or more elements). Curiously, while total correlation monotonically increases as \mathbf{X} transitions from randomness to synchrony, the dual total correlation is low both for totally random, and totally synchronized systems, peaking when \mathbf{X} is dominated by “shared” information.

Rosas et al. [24], propose that the difference between $TC(\mathbf{X})$ and $DTC(\mathbf{X})$ (first explored by James and Crutchfield as the *enigmatic information* [26]) could provide a measure of the overall balance between *redundancy* and *synergy* in multivariate systems: if $TC(\mathbf{X}) > DTC(\mathbf{X})$, then the global constraints on the system dominate and force a redundant dynamic, while if $TC(\mathbf{X}) < DTC(\mathbf{X})$ the system is dominated by information that is both shared, but not redundant. Rosas et al., rechristen this measure the *organizational information*:

$$\Omega(\mathbf{X}) = TC(\mathbf{X}) - DTC(\mathbf{X}) \quad (7)$$

While O-information has been applied in a variety of contexts (such as to questions about the aging brain [22], information flow in neuronal circuits [43], and even music composition [17]), there remains considerable uncertainty around how “synergy” should be intuitively understood. To help elucidate the answer, we relate O-information to the original measure of integration/segregation balance proposed by Tononi, Sporns, and Edelman: the TSE complexity [9] and show that a geometric interpretation of the O-information exists that brings with it a novel perspective on redundancy and synergy.

The TSE-complexity admits two formulations:

$$TSE(\mathbf{X}) = \sum_{i=1}^{\lfloor n/2 \rfloor} \mathbb{E}[I(\mathbf{X}^\gamma; \mathbf{X}^{-\gamma})]_{|\gamma|=i} \quad (8)$$

$$= \sum_{i=1}^N \left(\frac{i}{N} TC(\mathbf{X}) - \mathbb{E}[TC(\mathbf{X}^\gamma)] \right)_{|\gamma|=i} \quad (9)$$

The first (Eq. 8) defines the TSE complexity as the average mutual information between the pairs of every possible bipartition of the system \mathbf{X} . For every integer i between 1 and $\lfloor n/2 \rfloor$, we compute all possible subsets of \mathbf{X} with i elements (notated by \mathbf{X}^γ) and compute the mutual information between that set and its complement ($\mathbf{X}^{-\gamma}$). The second equation (Eq. 9) provides an alternative interpretation: the TSE complexity quantifies the difference, at every scale, between the “expected” integration of the scale if the system were fully integrated, and the actual integration of that scale (calculated as the average total correlation of every subset of size k). In this interpretation, the TSE complexity is highest when the smallest scales are relatively dis-integrated, but the

macro-scales are relatively *more* integrated. This balance of integration and segregation is emblematic of TSE “complexity.” For a visualization of the TSE complexity calculation as the difference between the expected and empirical values, see Figure 1.

Computing the full TSE complexity itself requires analyzing every possible subsystem (or bipartition) of \mathbf{X} : an insurmountable task for all but the smallest networks, as the combinatorics grow super-exponentially. A useful approximation is to look only at the second-to-top “layer” of the full TSE complexity summation, which only requires finding the average total correlation for the N sets \mathbf{X}^{-i} (where \mathbf{X}^{-i} is every $X \in \mathbf{X}$ excluding X_i). We refer to this measure as the *description complexity* of \mathbf{X} [10, 44]. Formally:

$$C(\mathbf{X}) := TC(\mathbf{X}) - \frac{TC(\mathbf{X})}{N} - \mathbb{E}[TC(\mathbf{X}^{-i})] \quad (10)$$

The definition of $C(\mathbf{X})$ as successive pruning of information. $TC(\mathbf{X})$ is the total integration of \mathbf{X} . $-TC(\mathbf{X})/N$ is *expected* decrease in integration associated with a single element (on average), and $-\mathbb{E}[TC(\mathbf{X}^{-i})]$ is the *actual* decrease in integrated associated with removing every element on its own. C , then, computes the difference between the expected decrease in integration associated with removing a single node and the actual decrease. C has several obvious conceptual parallels with the DTC and there is indeed an analytic relationship between DTC and C (for proof, see SI):

$$DTC(\mathbf{X}) = N \times C(\mathbf{X}) \quad (11)$$

This result was independently derived in [45]. The relationship between DTC and C allows us to rewrite the O-information purely in terms of total correlations:

$$\Omega(\mathbf{X}) = TC(\mathbf{X}) - N \times C(\mathbf{X}) \quad (12)$$

$$= (2 - N)TC(\mathbf{X}) + \sum_{i=1}^N TC(\mathbf{X}^{-i}) \quad (13)$$

This allows us to re-conceptualize redundancy- and synergy-dominance in terms of just redundancy: synergistic information is information that is redundantly present in large ensembles of elements considered jointly but not in any subset of those ensembles. This is conceptually very similar to the definition of synergy provided by the partial information decomposition [31], which defines synergy in terms of redundant information shared by higher-order collections of elements. We can also propose a geometric interpretation of the sign of the O-information: based on Eqs. 7 and 12, we can see that $\Omega(\mathbf{X}) < 0 \iff TC/N < C$ and $\Omega(\mathbf{X}) > 0 \iff TC/N > C$. This means that a system \mathbf{X} is *synergy-dominated* if the removal of a single element (on average) decreases the integration of the remaining $N - 1$ elements

more than would be expected in the null case of a totally integrated system. The two possible cases (redundancy-dominated, with $\Omega > 0$ and synergy-dominated, with $\Omega < 0$) are visualized and discussed in the context of the TSE complexity in Figure 1.

Another heuristic approximation of the TSE complexity is the sum of the total correlation and dual total correlation. Following the notation from Rosas et al.:

$$\Sigma(\mathbf{X}) = TC(\mathbf{X}) + DTC(\mathbf{X}) \quad (14)$$

James et al. previously termed this measure the *exogenous information* and described it as a “very mutual information”: quantifying all of the shared dependencies between each single variable and every other subset of the system:

$$\Sigma(\mathbf{X}) = \sum_{i=1}^N I(X_i; \mathbf{X}^{-i}) \quad (15)$$

Given the obvious similarity to Eq. 8, Rosas et al., hypothesized that $\Sigma(\mathbf{X}) \propto TSE(\mathbf{X})$, which was verified to hold in simple simulations with small N [24]. By leveraging the Gaussian assumptions here, we can empirically estimate the correlation between TSE and exogenous information and assess how well the relationship holds as N gets large. Figure 2 confirms the strong correlations between TSE complexity with both $TC+DTC$ and DTC alone. These correlations hold over a range of subset sizes, from three to fifteen elements.

II. RESULTS

We set out to identify subsystems (subsets of dynamically interacting elements) that express negative O-information (synergy) in the human brain. Leveraging Gaussian assumptions [35] (see Methods), multivariate information theoretic measures can be estimated from covariance (correlation) matrices expressing empirically recorded functional connectivity (FC). We computed long-time averages of FC derived from two normative samples of human resting-state fMRI, the Human Connectome Project (main data set; [46]) and an open-source multimodal MRI dataset for Microstructure-Informed Connectomics (MICA-MICs; replication data set; [47]). For both data sets we computed a single FC matrix (HCP: 95 participants, 4 runs each; MICA-MICs: 50 participants, 1 run each). Both FC covered the entire cerebral cortex parcellated into a common set of 200 nodes [48] and node time series were derived from BOLD signals after performing global signal regression, which removes signal components that are common to all nodes in the system, i.e. globally redundant (Fig. SI1).

Computing O-Information on the full-size 200-node FC matrix results in positive quantities for both data sets

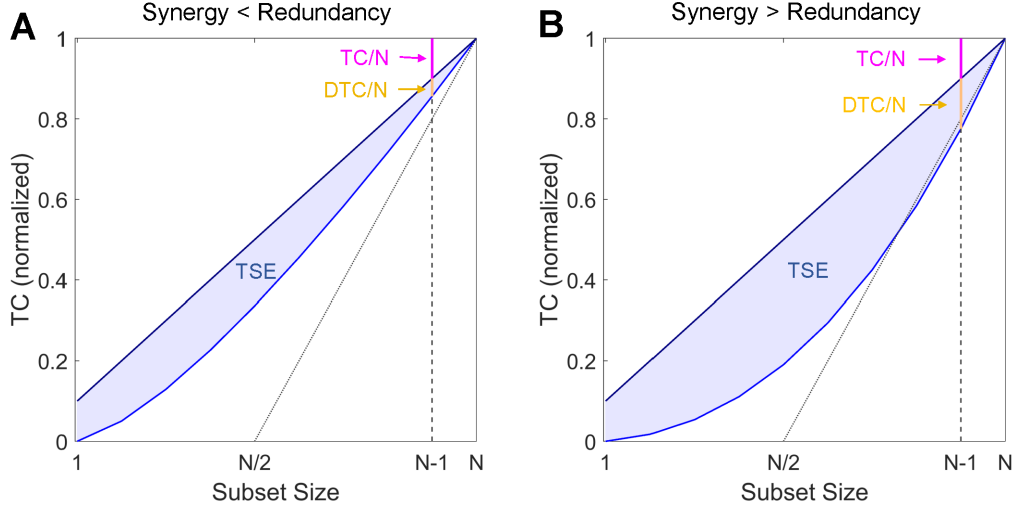


FIG. 1. Understanding O-information in the context of the TSE Complexity. The TSE Complexity provides a system-wide summary statistic of how integrated the system is at every scale. The O-information can be understood as measuring how sensitive the global integration is to the removal of single elements (on average). **A:** The panel shows a TSE curve for a low-synergy system: $TC(\mathbf{X})/N > DTC(\mathbf{X})/N$, so $\Omega(\mathbf{X}) > 0$. The erasure of any single element, on average, does not change the overall integration of the remaining $(N - 1)$ elements more than would be expected in the null case. **B:** The panel shows the case where $TC(\mathbf{X})/N < DTC(\mathbf{X})/N$, so $\Omega(\mathbf{X}) < 0$ and the system is “synergy dominated”. Intuitively, this can be understood by recognizing that, on average, the removal of any of the N elements causes a large decrease in the integration among the remaining $(N - 1)$ elements.

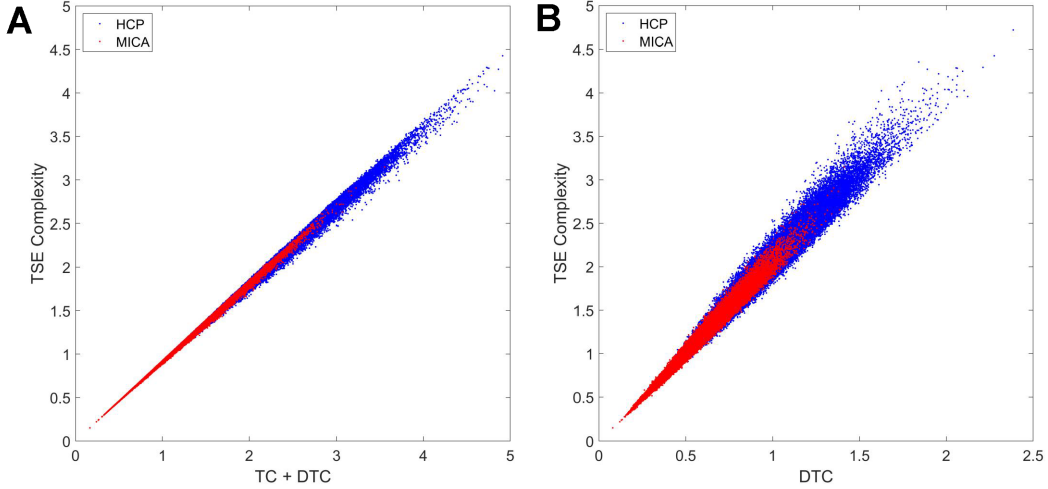


FIG. 2. Approximating TSE complexity with total correlation and dual total correlation. Data are from 100,000 randomly selected subsets of 10 nodes (blue: HCP data; red: MICA data), with TSE complexity computed exactly, by sampling all subsystems. **(A)** Sum of TC+DTC versus TSE complexity; HCP: $R = 0.998, p = 0$; MICA: $R = 0.999, p = 0$. **(B)** DTC versus TSE; HCP: $R = 0.982, p = 0$; MICA: $R = 0.992, p = 0$.

(HCP: $\Omega = 79.16$ nats; MICA: $\Omega = 46.69$ nats), indicating that the full structure is redundancy-dominated, which might potentially obscure the presence of higher-order, synergistic correlations. We asked if smaller subsets of nodes were present within the full-size FC that generated synergy, or negative O-information. Random sampling of small subsets (between 3 and 16 nodes) indeed yields abundant subsets that express negative O-

information (Fig 3A). Their relative abundance declines rapidly with growing subset size, reflecting the increasing dominance of redundant information and exhaustive capture of unique information. While synergistic subsets account for rapidly diminishing fractions of all subsets, their total number can be non-negligible (10-node subsets: 0.41 percent and 9.23×10^{13} , respectively). In a large random sample of 10-node subsets, the O-

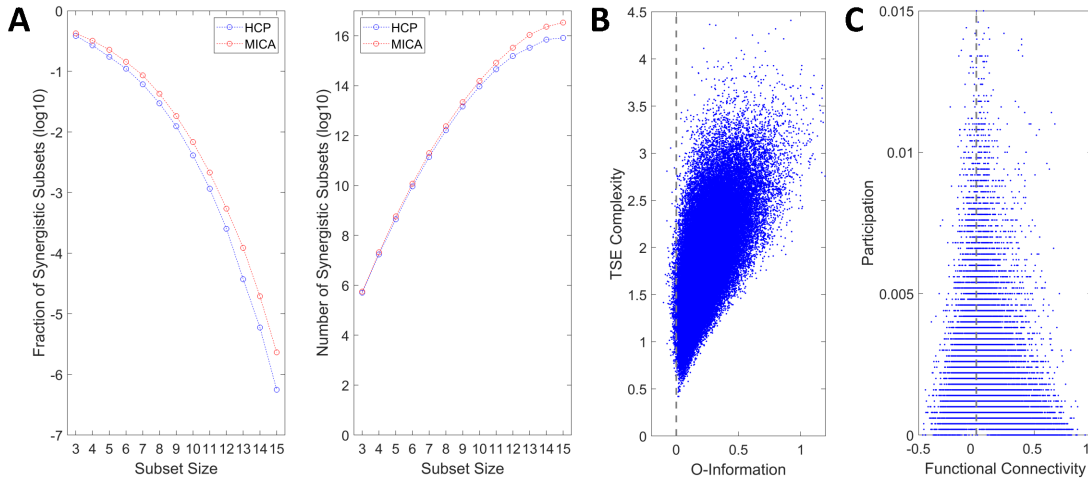


FIG. 3. Information measures computed from randomly sampled 10-node subsets. (A) Fraction (left) and number (right) of subsets with negative O-information, obtained by randomly sampling subsets from the HCP (blue) and MICA (red) FC matrix. Fraction and number estimated from samples of 5,000 (3-12 nodes) or 200 (13-15 nodes) subsets with negative O-information. As the size of the subset grows, the fraction expressing an overall synergy-dominated structure (negative O-information) drops precipitously, while their absolute number continues to climb due to combinatorics. (B) The relation between O-information and TSE complexity in 100,000 randomly sampled 10-node subsystems (HCP data). While very few randomly-sampled sets have negative O-information (see panel A), TSE complexity generally increases with the strength of the dependencies visible to the O-information ($R = 0.642, p = 0$). (C) The participation quantifies, for each node pair, how often they are encountered as part of a subset with negative O-information (10 nodes, 5,000 random samples, HCP data). The plot shows the relation of the participation against the FC, with each data point representing one of the 19,900 unique node pairs. Node pairs with strong mutual FC (positive or negative) are rarely encountered as part of the same synergistic subset, while node pairs that are more frequently encountered tend to show weak FC. Spearman's rho between absolute FC and participation: $\rho = -0.504, p = 0$.

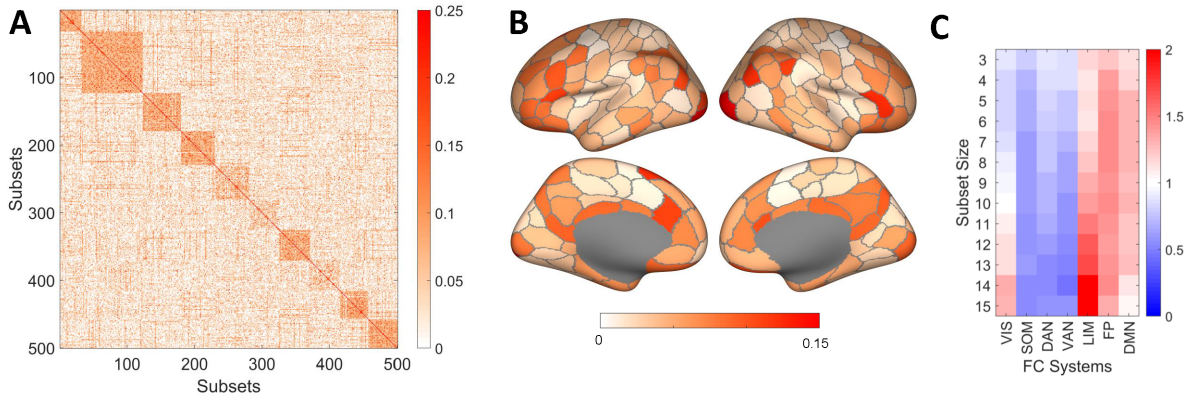


FIG. 4. Topography and functional specialization of randomly sampled synergistic subsets in the brain. Data in panels A and B was derived from a random sample of 100,000 synergistic 10-node subsets (HCP data). (A) Drawing random sub-samples of 500 subsets, we computed their Jaccard similarity, capturing the number of nodes in common between each subset pair. The similarity matrix was clustered using the kmeans algorithm, iterating between 2 and 30 clusters, with 10,000 repetitions. Optimal cluster quality was determined using the 'silhouette' criterion on the resulting cluster assignments. Random samples consistently yielded around 9-11 optimal clusters, with one example (10 clusters) shown in this panel. A Jaccard similarity of 0.25 corresponds to two subsets having 4 out of 10 nodes in common. (B) Frequency of individual node participation across 100,000 synergistic subsets, displayed on a surface rendering of the cerebral cortex indicating the boundaries of the 200 nodes used for constructing the FC matrix. (C) Each of the 200 nodes is affiliated with one of 7 canonical functional systems [49]. Frequency of participation of individual nodes in synergistic subsets (negative O-information, subset size ranging from 3 to 15 nodes) is aggregated (averaged) for each functional system. The plot displays the ratio of empirical frequency over the expected frequency if nodes were selected by chance. A ratio > 1 or < 1 indicates that the system is over-represented or under-represented, respectively, in synergistic subsets. Sample sizes identical to those used in Fig 4A.

information is positively correlated with TSE complexity (Fig 3B; $\rho = 0.642$, $p = 0$; HCP data). Focusing on a separate random sample of 5000 10-node subsets with negative O-information, we asked if the frequency with which pairs of nodes participate in such subsets is related to their pairwise FC. Indeed, the absolute pairwise FC is strongly negatively correlated with the frequency of participation in synergistic subsets ($\rho = -0.504$, $p = 0$, HCP; $\rho = -0.485$, $p = 0$, MICA, HCP; Fig 3C). This indicates that strongly positive or negative FC between two nodes makes their joint inclusion in a synergistic subset unlikely, while node pairs with low FC magnitude could either be truly disintegrated, or participating in a highly synergistic subsystem.

Participation of nodes in randomly sampled synergistic subsets varies systematically across the cortex. Over a large random sample of 100,000 10-node subsets, all nodes participate at least once, with several nodes participating in more than 10,000 distinct synergistic subsets. Hence, the complete repertoire of co-expressed synergistic subsets covers the entire cortex, with some overlap between subsets, centered on high-participation nodes that form “focal points” or clusters (Fig 4A). Projecting the participation of individual nodes (brain regions) onto the cortical surface shows significant consistency between HCP (Fig 4B) and MICA data (Fig SI4) (the two maps are correlated with $\rho = 0.579$, $p = 2.5 \times 10^{-19}$, between the two data sets). Functional systems [49] distribute unevenly as well, with highest frequencies of participation found in the frontoparietal (FP) system, for synergistic subsets of 10 nodes (HCP: Fig 4C; MICA: Fig SI2C). For larger subset sizes, participation of limbic (LIM) regions dominates over FP regions.

Combinatorics prevent exhaustive exploration of subsets of even modest sizes, and the random sampling strategy employed so far is likely to miss subsets that express maximal synergy. To identify subsets with maximally negative O-information (maximal synergy), we used an optimization algorithm based on simulated annealing (references and details are contained in the Methods section). Multiple runs of the algorithm yielded consistent and highly similar outcomes (Fig SI3), indicating convergence of the optimization while again highlighting the existence of a large reservoir of non-identical (degenerate) subsets, all expressing highly negative O-information. Deploying this algorithm while varying subset sizes between 3 and 30 nodes, we identified large numbers of subsets that express highly negative O-information, for subset sizes 3-24 nodes (HCP; Fig. 5A) and 3-27 nodes (MICA; Fig. SI4). No synergistic subsets are found for subset sizes greater than 27 nodes, as redundancy starts to overwhelm the unique informational contributions of individual nodes at larger subset sizes.

Minimal O-information was achieved for subsets comprising approximately 10 nodes for both data sets. Mapping subsets of nodes expressing near minimal O-information onto a surface plot of the cerebral cortex reveals consistent topography. Fig. 5B shows the fre-

quency with which individual cortical parcels (nodes) were identified across 5000 runs of the optimization algorithm, yielding 4021 unique solutions (HCP Fig. 5B; 4166 unique solutions for MICA data, Fig SI4B). Brain-wide nodal frequencies are significantly correlated across HCP and MICA data sets (Spearman’s $\rho = 0.522$, $p = 2.2 \times 10^{-15}$). When mapping these nodal frequencies to seven canonical resting-state functional systems [49], we find that each of these seven systems contributes, but to different extent. In HCP data, for optimally synergistic 10-node subsets, the visual, frontoparietal and default mode networks are over-represented, while only the FP system appears over-represented in the MICA data; Fig SI5).

The nature of negative O-information (synergy) requires that individual nodes make largely unique (non-redundant) contributions to the multivariate information metric. This suggests that nodes derived from different, informationally distinct (intrinsically redundant, but extrinsically non-redundant) functional communities or systems might be favored as constituents of synergistic subsets. To test this hypothesis, we created sets of 20,000 randomly sampled subsets that were comprised of nodes derived from between 1 and all 7 canonical functional systems (HCP, Fig. 5C; MICA, Fig. SI4C). The mean O-information, across all randomly chosen subsets, was found to be positive regardless of how many FC systems were included in the subsets. For samples derived from just 1 FC system, the O-information was most positive (i.e. subsets were most redundancy-dominated) for visual, somatomotor and attention systems, and they were least redundancy-dominated for default, frontoparietal and limbic systems. Importantly, the mean O-information decreased, and the fraction of synergistic subsets increased, as subsets were sampled from larger numbers of canonical systems. No subset derived from a single functional system was capable of expressing synergy. Subsets spanning 6 or 7 canonical systems were most likely to express synergy, as indexed by the fraction of negative O-information encountered in the sample. The finding supports the notion that dividing the brain into canonical functional systems prioritizes grouping nodes by redundant over synergistic information, hence missing a potentially important substrate for neural computation.

III. DISCUSSION

In this paper, we have shown how the O-information [24], a measure of higher-order interactions in multivariate data, can reveal synergistic ensembles of brain regions that are invisible to bivariate functional connectivity analyses. Our primary theoretical result is to provide a geometric interpretation of the O-information that unifies multiple disparate measures of multivariate information sharing into a single framework, built around the Tononi-Sporns-Edelman complexity [9]. By re-writing

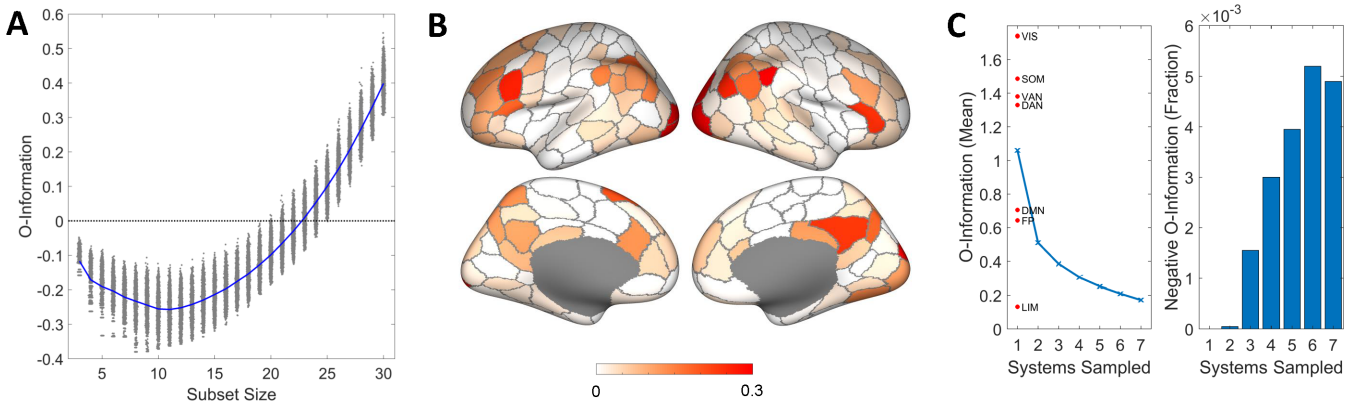


FIG. 5. O-Information, brain topography and functional specialization of optimally synergistic subsets identified by simulated annealing All panels show data from the HCP sample. **(A)** Annealing was carried out 5,000 times for each subset size. plot shows O-information for each optimized subset (gray dots) and their mean (blue line). Note that annealing fails to converge onto any synergistic subsets for subsets containing more than 24 nodes. Optimally negative O-information is achieved for subsets between 8 and 12 nodes. **(B)** Frequency of individual node participation across optimally synergistic 10-node subsets (4021 unique subsets out of 5,000 annealing runs), displayed on a surface rendering of the cerebral cortex (cf. Fig 4B). **(C)** Mean O-information (left) and fraction of synergistic subsets (right) encountered in samples of 20,000 subsets that contained nodes belonging to between 1 and 7 canonical FC systems (HCP data). The mean O-information for samples obtained exclusively from each of the 7 FC systems is indicated (red dots).

$\Omega(\mathbf{X})$ in terms of the total correlation between multiple subsets of \mathbf{X} , we find that “synergy” occurs when removing any single element causes the system to become less integrated (more so than would be expected if structure was uniformly distributed over \mathbf{X}). In this sense, synergy captures how the “whole” can be greater than the sum of its parts [50]. Applied to two separate fMRI brain data sets we find that synergistic subsets of brain regions are ubiquitous and abundant, comprising between 3 and 25 regions and extending over the entire cerebral cortex. While redundant interactions dominate functional connectivity at larger subset sizes, the application of multivariate information measures demonstrates a previously hidden repertoire of synergistic ensembles, each integrating diverse and distinct sources of information.

The theoretical results, including the geometric interpretation of the O-information presents a new, intuitive approach to understanding the often un-intuitive notion of synergy. By re-writing $\Omega(\mathbf{X})$ in terms of only sums and differences of total correlations, we can see that synergy can be approximately understood as that “integration” that is present in the whole but not smaller subsets (in this case, the N subsets created by removing each X_i). This intuition is conceptually similar to the formal definition of synergy from the partial information decomposition framework [31], which computes synergy as the information “left over” when everything accessible in simpler combinations of sources has been accounted for. The exclusive use of total correlations also allows us to consider the O-information purely in terms of Kullback-Leibler divergences from independent to joint probability distributions (Eq. 5). This shows us that all of these mea-

sures can be understood in the context of “inferences” about structure (relative to a disintegrated prior). In the context of synergy, the “extra” information in the joint state is information *about* something: specifically about the relative likelihood of a configuration with respect to the maximum entropy case.

When randomly sampling subsystems in two datasets (HCP and MICA), we found a large number of synergy-dominated ensembles distributed throughout the brain. Recent work by Luppi et al., [21] proposed a “synergistic core” to the human brain where complex processing occurs. While we found that there is significant overrepresentation of specific regions (including portions reported by Luppi et al., such as prefrontal cortex, occipital pole, the precuneus, and cingulate regions), synergy-dominated subsystems could include any region of cortex: regions contributing to synergistic subsets are very widely distributed. Almost every region contributed to at least some synergistic ensembles, although some regions contribute more reliably than others. This suggests that synergy is a widespread property of multivariate information emerging from resting-state brain activity.

Interestingly, the randomly sampled ensembles that were most likely to be synergy dominated were those that involved nodes that spanned multiple canonical subsystems, while sets of regions all within one system were strongly dominated by redundancy (Fig. 5C). This would be consistent with the hypothesis that functional connectivity, when viewed entirely as bivariate interaction, is largely sensitive to redundant, but insensitive to synergistic, dependencies between brain regions. Consequently, the functional connectivity matrix is not a “complete” map of the statistical structure in a dataset, but only of

dependencies characterized by redundancy. This is consistent with findings from Ince [51] and Finn and Lizier [52] who argued that bivariate correlations are intrinsically redundancy-dominated. Higher-order synergies represent, in a sense, a kind of “shadow structure” and consequently missed by network-focused approaches that omit higher-order interactions. This hypothesis finds some support in [21], who found that the distribution of synergies was anticorrelated with the functional connectivity network structure, while the distribution of redundancies was positively correlated.

Given the novelty of tools like the O-information, the significance of these synergistic dependencies remains almost entirely unknown, although the small number of studies to date suggest intriguing patterns. One study found alterations to the redundancy/synergy bias across the human lifespan [22], while other studies have suggested that loss of consciousness induced by propofol is associated with decreased synergistic dynamics [20]. Future avenues of work include deeper analyses of how higher-order dynamics change between rest and task conditions, in cases of psychopathology or brain injury and non-human animals. We should note that, in the context of the O-information, synergy is not necessarily a “causal” measure: in related contexts, synergy has been discussed as a measure of “computation” in neural circuits [13–15, 53], although it remains unexplored how exactly these two approaches relate to each other. The O-information measures instantaneous, higher-order correlation structures, while the work by Sherill et al., is done in the context of information dynamics [25]. Future research may explore how a synergistic correlation structure might facilitate computations within the system over time.

In addition to the insights into synergy specifically, the results presented here also have implications for researchers interested in multivariate information theoretic analyses. For example, the TSE complexity has long been an object of theoretical interest [45], but the intractable combinatorics have limited its applicability in empirical data (although its use is not unheard of [54]). The finding that the exogenous information $\Sigma(\mathbf{X}) \propto TSE(\mathbf{X})$ for reasonably large N (first reported in [24]), even more so than the original heuristic C , opens the door to applications application in experimental neuroscience.

In a broader scientific context, our work contributes to the increasing interest in higher-order interactions, beyond the standard, pairwise network model [8, 55]. The information-theoretic approach (such as the work reported here, as well as in [17, 20, 21, 43, 53, 56]) is based largely on a statistical inference, while alternative frameworks based on simplicial complexes, algebraic topology, and hypergraphs has been developed largely in parallel [7, 34, 57–60]. How these different mathematical frameworks relate to each other remains an open question, and the potential for a more unified approach to understanding higher-order interactions both in terms of topology and statistical inferences is an alluring promise.

The optimization of maximally synergistic subsets via simulated annealing can be thought of as an attempt to find a maximally efficient, dimensionally-reduced representation of a potentially large data set: when modeling a system, it is generally desirable to capture as many statistical dependencies as possible with the fewest required degrees of freedom. By finding a representation that incorporates synergies while simultaneously pruning redundant information that would be “double counted”, we can attempt to build the most computationally efficient model of a system under study [61, 62]. While dimensionality reduction and feature selection algorithms are widespread in many computational sciences, a rigorous treatment of the ways that synergistic and redundant information can inform the analysis of brain dynamics and functional networks remains a space of active development (for an example, see [62, 63]).

The O-information scales far more gracefully than related measures of synergistic information (such as the partial information decomposition, which is practically impossible to apply to systems larger than 5 elements [64]). However the combinatorics associated with assessing every possible subsystem becomes intractable as the system size grows, an issue first noted for the TSE complexity. In standard functional and effective network research, it is common to compute all pairwise interactions (which only grows with N^2), and then filter out spurious edges as needed [63]. While this may be possible for very small subsystems, it is intractable for larger ones. If one can pre-select a set of elements, then the computation of O-information is trivial up to hundreds of items. However, the requirement to select subsets of interest can itself be computationally intensive and time-consuming. Consequently heuristic measures such as optimization, random sampling, or pre-filtering subsystems to exclude collections of elements will be required.

In this article, we demonstrate how an information-theoretic measure of multivariate interactions (the O-information or synergy) can be used to uncover higher-order interactions in the human brain dynamics. We analytically show that the O-information can be related to an older measure of systemic complexity, the TSE complexity, and from this derive a novel geometric interpretation of redundancy- and synergy-dominated systems. With a combination of random sampling and optimization, we show that a large number of subsystems displaying synergistic dynamics exist in the human brain and that these systems form a highly distributed “shadow structure” that is entirely overlooked in standard, bivariate functional connectivity models. We conclude that the space of higher-order interactions in the human brain represents a large, and under-explored area of study with a rich potential for new discoveries and experimental work.

IV. METHODS

A. Gaussian Information Theory

In this paper, we focus on higher-order information sharing in fMRI BOLD signals. Prior work has established that BOLD data is well-modeled by multivariate Gaussian distributions [65, 66] and that more complex and highly-parameterized models provide little additional benefit [67]. While information theory was originally formalized in the context of discrete random variables, in the specific case of Gaussian random variables, closed-form estimators exist for almost all the standard information measures (for an accessible review, see [68] supplementary material). For a univariate, Gaussian random variable $X \sim \mathcal{N}(\mu, \sigma)$, the entropy (given in nats) is defined as:

$$H^{\mathcal{N}}(X) = \frac{\ln(2\pi e\sigma^2)}{2} \quad (16)$$

For a multivariate Gaussian random variable $\mathbf{X} = \{X_1, X_2, \dots, X_N\}$, the joint entropy is given by:

$$H^{\mathcal{N}}(\mathbf{X}) = \frac{\ln[(2\pi e)^N |\Sigma|]}{2} \quad (17)$$

where $|\Sigma|$ refers to the determinant of the covariance matrix of \mathbf{X} . The bivariate mutual information (nats) between X_1 and X_2 is:

$$I^{\mathcal{N}}(X_1; X_2) = \frac{-\ln(1 - \rho^2)}{2} \quad (18)$$

where ρ is the Pearson correlation coefficient between X_1 and X_2 . Note that, since the mutual information is a function of ρ for Gaussian variables, this special case of mutual information is **not** generally sensitive to non-linear relationships in the data in the way that non-parametric estimators are. Finally, the Gaussian estimator for total correlation is:

$$TC^{\mathcal{N}}(\mathbf{X}) = \frac{-\ln(|\Sigma|)}{2} \quad (19)$$

From these, it is possible to calculate all of the measures described above (dual total correlation, description complexity, O-information, and TSE complexity) for multivariate Gaussian variables. While the assumption of linearity that comes with a parametric Gaussian model can be limiting, the standard technique for assessing functional connectivity (the Pearson correlation coefficient) makes identical assumptions, so our work is consistent with assumptions made when applying standard approaches to FC analysis.

B. Datasets

Two independent fMRI resting state data sets were employed in the empirical analyses, one derived from the Human Connectome Project (HCP data; [46]) and the other from a recently published open-source repository (MICA; [47]). The HCP data, derived from a set of 100 unrelated subjects, have been used in several previous studies (for more detailed description see [69]). All participants provided informed consent, and the Washington University Institutional Review Board approved all of the study protocols and procedures. A Siemens 3T Connectom Skyra equipped with a 32-channel head coil was used to collect data. Resting-state functional MRI (rs-fMRI) data was acquired during four scans on two separate days. This was done with a gradient-echo echo-planar imaging (EPI) sequence (scan duration: 14:33 min; eyes open). Acquisition parameters of TR = 720 ms, TE = 33.1ms, 52° flip angle, isotropic voxel resolution = 2 mm, with a multiband factor of 8 were used for data collection. A parcellation scheme covering the cerebral cortex developed in ref. [48] was used to map functional data to 200 regions. This parcellation can also be aligned to the canonical resting state networks found in ref. [49].

Of the 100 unrelated subjects considered in the original dataset, 95 were retained for inclusion in empirical analysis in this study. Exclusion criteria were established before the present study was conducted. They included the mean and mean absolute deviation of the relative root mean square (RMS) motion across either four resting-state MRI scans or one diffusion MRI scan, resulting in four summary motion measures. Subjects that exceeded 1.5 times the interquartile range (in the adverse direction) of the measurement distribution in two or more of these measures were excluded. Following these criteria, four subjects were excluded. Due to a software error during diffusion MRI processing, one additional subject was excluded. The remaining 95 subjects were 56% female, had a mean age of 29.29 ± 3.66 , and an age range of 22 to 36.

The MICA dataset includes 50 unrelated subjects, who also provided written informed consent. The study was approved by the Ethics Committee of the Montreal Neurological Institute and Hospital. Resting state data was collected in a single scan session using a 3T Siemens Magnetom Prisma-Fit with a 64-channel head coil. Resting state scans lasted for 7 minutes during which participants were instructed to look at a fixation cross. Imaging was completed with an EPI sequence, and acquisition parameters of TR = 600ms, TE = 48ms, 52° flip angle, isotropic voxel resolution = 3 mm, and multiband factor 6. The parcellation used in this dataset was the same as the one used for the HCP data (described above).

C. Preprocessing

Minimal preprocessing of the HCP rs-fMRI data followed these steps [70]: 1) distortion, susceptibility, and motion correction; 2) registration to subjects' respective T1-weighted data; 3) bias and intensity normalization; 4) projection onto the 32k_fs_LR mesh; and 5) alignment to common space with a multimodal surface registration [71]. The preprocessing steps described produced an ICA+FIX time series in the CIFTI grayordinate coordinate system. Two additional preprocessing steps were performed: 6) global signal regression and 7) detrending and band pass filtering (0.008 to 0.08 Hz) [72]. After confound regression and filtering, the first and last 50 frames of the time series were discarded, resulting in a final scan length of 13.2 min (1,100 frames).

Preprocessing of the MICA dataset was performed as described in ref. [47] for resting state data. Briefly, the data was passed through the Micapipe [73] processing pipeline, which includes motion and distortion correction, as well as FSL's ICA FIX tool trained with an in-house classifier. Time series were projected to each subject's FreeSurfer surface, where nodes were also defined. Further details about the processing pipeline can be found in [73]. The data was global signal regressed in addition to the other preprocessing steps described in this pipeline.

For calculating the covariance matrix used in computing O-information, total correlation and dual total correlation, the functional data from all scans and all subjects were combined to create a single COV or FC matrix. Aggregation was carried out by appending the nodal time series across all subjects and runs and then calculating a single Pearson correlation for each node pair. An alternative approach (taking the mean over the single-run, single-subject COV/FC matrices) yielded virtually identical results. Following preprocessing and using the common 200-node parcellation of cerebral cortex, the mean COV/FC matrices for the HCP and MICA data sets were highly correlated ($R = 0.851, p = 0$).

D. Random Sampling and Optimization

Subsets of regions were selected from the full-size (200 nodes/regions) FC matrices in two ways, by random sampling and by search through optimization. Random sampling is simple to implement but because of the vast repertoire of potential subsets ($\binom{N}{k}$) it cannot fully disclose the extent of variations in informational measures present in the data. Instead, search under an objective function (optimization) can guide exploration to specific sub-spaces enriched in subsets with distinct informational signatures.

To perform optimizations we implemented a variant of

simulated annealing [74]. As objectives we chose multi-variate informational measures such as the O-information (OI), total correlation (TC), and dual total correlation (DTC), which could be maximized or minimized. Each run of the simulated annealing algorithm was carried out in one FC matrix and for one subset size. We carried out 5000 runs, with subset sizes ranging from 3 to 30 nodes. A random selection of nodes was chosen according to the given subset size to initiate each run. The corresponding covariance matrix was extracted from the full COV/FC and used to compute the information theoretic metric of interest. The composition of the subset was then varied and variations were selected under the objective function. Annealing operates by selecting variations stochastically, depending on a temperature parameter that determines the amount of noise permitted in the selection process. Initially, the temperature is high, resulting in the somewhat random exploration of the landscape. As the temperature is lowered, the optimization becomes more deterministic, focusing more and more on local gradient descent. For each run the algorithm proceeded for a maximum of 10,000 steps. At each step, a new set of nodes was generated by randomly replacing nodes, with the number determined by a normal distribution (frequencies of 1, 2 and 3 element flips were 0.68, 0.27 and 0.04, respectively). A new covariance matrix was computed for the new set of nodes and the objective function was calculated for that set. The set was retained if its cost was lower than the current set or if a random number drawn from the uniform distribution between 0 and 1 was less than $\exp(-((C_n - C_c)/T_c))$, where C_n is the cost of the new set of nodes, C_c is the cost of the current set of nodes and T_c is the current temperature. At each step, the current temperature decays to a fraction of the initial temperature, as a function of the number of steps completed:

$$T_c(h) = T_0 T_{exp}^h \quad (20)$$

where T_c is the current temperature, T_0 is the initial temperature (set to $T_0 = 1$), T_{exp} governs the steepness of the temperature gradient, and h is the current iteration step. By decreasing the temperature at every step, the algorithm becomes progressively more deterministic.

Acknowledgements

T.F.V. and M.P. are supported by the NSF-NRT grant 1735095, Interdisciplinary Training in Complex Networks and Systems. The funders had no role in study design, data collection and analysis, decision to publish, or preparation of the manuscript.

- [3] O. Sporns and R. Kötter, *PLOS Biology* **2**, e369 (2004).
- [4] D. J. Watts and S. H. Strogatz, *Nature* **393**, 440 (1998).
- [5] S. Fortunato, *Physics Reports* **486**, 75 (2010).
- [6] R. F. Betzel, arXiv:2011.06723 [q-bio] (2020), arXiv: 2011.06723.
- [7] F. Battiston, G. Cencetti, I. Iacopini, V. Latora, M. Lucas, A. Patania, J.-G. Young, and G. Petri, *Physics Reports Networks beyond pairwise interactions: Structure and dynamics*, **874**, 1 (2020).
- [8] F. Battiston, E. Amico, A. Barrat, G. Bianconi, G. Ferraz de Arruda, B. Franceschiello, I. Iacopini, S. Kéfi, V. Latora, Y. Moreno, M. M. Murray, T. P. Peixoto, F. Vaccarino, and G. Petri, *Nature Physics* (2021), 10.1038/s41567-021-01371-4.
- [9] G. Tononi, O. Sporns, and G. M. Edelman, *Proceedings of the National Academy of Sciences* **91**, 5033 (1994).
- [10] G. Tononi, G. M. Edelman, and O. Sporns, *Trends in Cognitive Sciences* **2**, 474 (1998).
- [11] G. Tononi and G. M. Edelman, *Brain Research Reviews* **31**, 391 (2000).
- [12] N. M. Timme, S. Ito, M. Myroshnychenko, S. Nigam, M. Shimono, F.-C. Yeh, P. Hottowy, A. M. Litke, and J. M. Beggs, *PLOS Computational Biology* **12**, e1004858 (2016).
- [13] S. P. Faber, N. M. Timme, J. M. Beggs, and E. L. Newman, *Network Neuroscience* **3**, 1 (2018).
- [14] S. P. Sherrill, N. M. Timme, J. M. Beggs, and E. L. Newman, *PLOS Computational Biology* **17**, e1009196 (2021).
- [15] S. P. Sherrill, N. M. Timme, J. M. Beggs, and E. L. Newman, *Network Neuroscience* **4**, 678 (2020).
- [16] T. Varley, O. Sporns, H. Scherberger, and B. Dann, *bioRxiv*, 2021.09.05.458983 (2021).
- [17] T. Scagliarini, D. Marinazzo, Y. Guo, S. Stramaglia, and F. E. Rosas, arXiv (2021).
- [18] F. E. Rosas, P. A. M. Mediano, H. J. Jensen, A. K. Seth, A. B. Barrett, R. L. Carhart-Harris, and D. Bor, *PLOS Computational Biology* **16**, e1008289 (2020).
- [19] T. Varley, O. Sporns, A. Puce, and J. Beggs, *PLOS Computational Biology* **16**, e1008418 (2020).
- [20] A. I. Luppi, P. A. M. Mediano, F. E. Rosas, J. Allanson, J. D. Pickard, R. L. Carhart-Harris, G. B. Williams, M. M. Craig, P. Finoia, A. M. Owen, L. Naci, D. K. Menon, D. Bor, and E. A. Stamatakis, *bioRxiv* (2020), 10.1101/2020.11.25.398081.
- [21] A. I. Luppi, P. A. M. Mediano, F. E. Rosas, N. Holland, T. D. Fryer, J. T. O'Brien, J. B. Rowe, D. K. Menon, D. Bor, and E. A. Stamatakis, *Nature Neuroscience*, 1 (2022).
- [22] M. Gatica, R. Cofré, P. A. Mediano, F. E. Rosas, P. Orio, I. Diez, S. P. Swinnen, and J. M. Cortes, *Brain Connectivity* (2021), 10.1089/brain.2020.0982.
- [23] A. I. Luppi, P. A. M. Mediano, F. E. Rosas, D. J. Harrison, R. L. Carhart-Harris, D. Bor, and E. A. Stamatakis, *Neuroscience of Consciousness* **2021** (2021), 10.1093/nc/niab027.
- [24] F. Rosas, P. A. M. Mediano, M. Gastpar, and H. J. Jensen, *Physical Review E* **100**, 032305 (2019).
- [25] J. T. Lizier, B. Flecker, and P. L. Williams, arXiv (2013), 10.1109/ALIFE.2013.6602430.
- [26] R. G. James, C. J. Ellison, and J. P. Crutchfield, *Chaos: An Interdisciplinary Journal of Nonlinear Science* **21**, 037109 (2011).
- [27] G. Deco, G. Tononi, M. Boly, and M. L. Kringelbach, *Nature Reviews Neuroscience* **16**, 430 (2015).
- [28] J. M. Shine, *Trends in Cognitive Sciences* **23**, 572 (2019).
- [29] A. I. Luppi, M. M. Craig, I. Pappas, P. Finoia, G. B. Williams, J. Allanson, J. D. Pickard, A. M. Owen, L. Naci, D. K. Menon, and E. A. Stamatakis, *Nature Communications* **10**, 1 (2019).
- [30] A. I. Luppi, R. L. Carhart-Harris, L. Roseman, I. Pappas, D. K. Menon, and E. A. Stamatakis, *NeuroImage* **227**, 117653 (2021).
- [31] P. L. Williams and R. D. Beer, arXiv (2010).
- [32] G. R. McGhee, *Short Courses in Paleontology* **4**, 87 (1991).
- [33] A. Avena-Koenigsberger, J. Goñi, R. Solé, and O. Sporns, *Journal of The Royal Society Interface* **12**, 20140881 (2015).
- [34] T. F. Varley, V. Denny, O. Sporns, and A. Patania, *Royal Society Open Science* **8**, 201971 (2021).
- [35] T. M. Cover and J. A. Thomas, *Elements of Information Theory* (2012).
- [36] C. E. Shannon, *Bell System Technical Journal* **27**, 379 (1948).
- [37] K. J. Friston, *Human Brain Mapping* **2**, 56 (1994).
- [38] E. van Diessen, T. Numan, E. van Dellen, A. W. van der Kooi, M. Boersma, D. Hofman, R. van Lutterveld, B. W. van Dijk, E. C. W. van Straaten, A. Hillebrand, and C. J. Stam, *Clinical Neurophysiology* **126**, 1468 (2015).
- [39] M. Ursino, G. Ricci, and E. Magosso, *Frontiers in Computational Neuroscience* **14** (2020), 10.3389/fn-com.2020.00045.
- [40] L. Barnett, S. D. Muthukumaraswamy, R. L. Carhart-Harris, and A. K. Seth, *NeuroImage* **209**, 116462 (2020).
- [41] O. Sporns, *Networks of the Brain* (2010).
- [42] S. A. Abdallah and M. D. Plumbley, *Physics Letters A* **376**, 275 (2012).
- [43] S. Stramaglia, T. Scagliarini, B. C. Daniels, and D. Marinazzo, *Frontiers in Physiology* **11** (2021), 10.3389/fphys.2020.595736.
- [44] O. Sporns, G. Tononi, and G. M. Edelman, *Behavioural Brain Research* **135**, 69 (2002).
- [45] N. Ay, E. Olbrich, N. Bertschinger, and J. Jost, ECCS'06 : Proceedings of the European Conference on Complex Systems 2006 (2006).
- [46] D. C. Van Essen, S. M. Smith, D. M. Barch, T. E. J. Behrens, E. Yacoub, and K. Ugurbil, *NeuroImage Mapping the Connectome*, **80**, 62 (2013).
- [47] J. Royer, R. Rodríguez-Cruces, S. Tavakol, S. Larivière, P. Herholz, Q. Li, R. V. d. Wael, C. Paquola, O. Benkarim, B.-y. Park, A. J. Lowe, D. Margulies, J. Smallwood, A. Bernasconi, N. Bernasconi, B. Frauscher, and B. C. Bernhardt, *An Open MRI Dataset for Multiscale Neuroscience*, Tech. Rep. (2021).
- [48] A. Schaefer, R. Kong, E. M. Gordon, T. O. Laumann, X.-N. Zuo, A. J. Holmes, S. B. Eickhoff, and B. T. T. Yeo, *Cerebral Cortex* **28**, 3095 (2018).
- [49] B. T. Yeo, F. M. Krienen, J. Sepulcre, M. R. Sabuncu, D. Lashkari, M. Hollinshead, J. L. Roffman, J. W. Smoller, L. Zöllei, J. R. Polimeni, B. Fischl, H. Liu, and R. L. Buckner, *Journal of Neurophysiology* **106**, 1125 (2011).
- [50] V. Griffith and J. Harel, arXiv:1311.7442 [cs, math] (2013).
- [51] R. A. A. Ince, arXiv (2017).
- [52] C. Finn and J. T. Lizier, *Entropy* **22**, 216 (2020).
- [53] T. F. Varley, arXiv (2022), 10.48550/arXiv.2202.12992.

- [54] N. M. Timme, N. J. Marshall, N. Bennett, M. Ripp, E. Lautzenhiser, and J. M. Beggs, *Frontiers in Physiology* **7** (2016), 10.3389/fphys.2016.00425.
- [55] F. E. Rosas, P. A. M. Mediano, A. I. Luppi, T. F. Varley, J. T. Lizier, S. Stramaglia, H. J. Jensen, and D. Marinazzo, *Nature Physics*, **1** (2022).
- [56] T. F. Varley and P. Kaminski, arXiv (2021).
- [57] A. E. Sizemore, J. Phillips-Cremins, R. Ghrist, and D. S. Bassett, *Network Neuroscience* **3**, 656 (2019).
- [58] M. Saggarr, O. Sporns, J. Gonzalez-Castillo, P. A. Bandettini, G. Carlsson, G. Glover, and A. L. Reiss, *Nature Communications* **9** (2018), 10.1038/s41467-018-03664-4.
- [59] J. Billings, M. Saggarr, J. Hlinka, S. Keilholz, and G. Petri, *Network Neuroscience* **5**, 549 (2021).
- [60] B. J. Stolz, T. Emerson, S. Nahkuri, M. A. Porter, and H. A. Harrington, *Journal of Physics: Complexity* **2**, 035006 (2021).
- [61] T. F. Varley and E. Hoel, *Philosophical Transactions of the Royal Society A: Mathematical, Physical and Engineering Sciences* **380**, 20210150 (2022).
- [62] P. Wollstadt, S. Schmitt, and M. Wibral, arXiv (2021).
- [63] L. Novelli, P. Wollstadt, P. Mediano, M. Wibral, and J. T. Lizier, *Network Neuroscience* **3**, 827 (2019).
- [64] A. J. Gutknecht, M. Wibral, and A. Makkeh, *Proceedings of the Royal Society A: Mathematical, Physical and Engineering Sciences* **477**, 20210110 (2021).
- [65] J. Hlinkaa, M. Paluša, M. Vejmelkaa, D. Mantini, and M. Corbetta, *NeuroImage* **54**, 2218 (2011).
- [66] R. Liégeois, B. T. T. Yeo, and D. Van De Ville, *NeuroImage* **243**, 118518 (2021).
- [67] M.-A. Schulz, B. T. T. Yeo, J. T. Vogelstein, J. Mourao-Miranada, J. N. Kather, K. Kording, B. Richards, and D. Bzdok, *Nature Communications* **11**, 4238 (2020).
- [68] J. T. Lizier, *Frontiers in Robotics and AI* **1** (2014), 10.3389/frobt.2014.00011.
- [69] O. Sporns, J. Faskowitz, A. S. Teixeira, S. A. Cutts, and R. F. Betzel, *Network Neuroscience* **5**, 405 (2021).
- [70] M. F. Glasser, S. N. Sotiropoulos, J. A. Wilson, T. S. Coalson, B. Fischl, J. L. Andersson, J. Xu, S. Jbabdi, M. Webster, J. R. Polimeni, D. C. Van Essen, M. Jenkinson, and WU-Minn HCP Consortium, *NeuroImage* **80**, 105 (2013).
- [71] E. C. Robinson, S. Jbabdi, M. F. Glasser, J. Andersson, G. C. Burgess, M. P. Harms, S. M. Smith, D. C. Van Essen, and M. Jenkinson, *NeuroImage* **100**, 414 (2014).
- [72] L. Parkes, B. Fulcher, M. Yücel, and A. Fornito, *NeuroImage* **171**, 415 (2018).
- [73] R. R. Cruces, J. Royer, P. Herholz, S. Larivière, R. Vos de Wael, C. Paquola, O. Benkarim, B.-y. Park, J. Degré-Pelletier, M. Nelson, J. DeKraker, C. Tardif, J.-B. Poline, L. Concha, and B. C. Bernhardt, *Micapipe: A Pipeline for Multimodal Neuroimaging and Connectome Analysis*, preprint (2022).
- [74] N. Metropolis, A. W. Rosenbluth, M. N. Rosenbluth, A. H. Teller, and E. Teller, *The Journal of Chemical Physics* **21**, 1087 (1953).